Determining the emittance using a wire scanner

Marleen Maxton, University of Heidelberg, Germany

Supervisor: Florian Burkart, DESY

September 7, 2022

Abstract

Characterization of the transverse beam parameters is a requirement for the operation of particle accelerators. In this report the transverse emittence and Courant–Snyder parameters were determined at the ARES linear electron accelerator at DESY by scanning the beam size versus the quadrupole strength. The beam size is determined by using a wire scanner and tomography methods. The measurement principles and results will be discussed in detail and a tool that was implemented to automate the measurement will be presented.

Contents

1 Introduction

The user application of particle accelerators often requires high brightness beams. Since the brightness is maximal for minimal transverse emitttance, it is desirable to determine and control this parameter. To characterize the emittance multiple methods can be used. A common method is to scan the transverse beam size against the quadrupole strength and calculated the emittance from the fit parameters for the resulting curve. Instead of changing the quadrupole strength multiple screen stations at different position can also be used to scan the beam size. As another method a mask can be inserted into the beam and imaged on a screen downstream to determine the emittance via a reconstruction algorithm. In this report we will focus on the quadrupole scan to determine the emittance.

The quadrupole scan was performed at the ARES accelerator at DESY. ARES is a normal-conduction RF linac with the purpose of providing low charge, ultrashort electron bunches. The beam size was determined using a wire scanner manufactured at the Paul-Scherrer-Institute (PSI) that is located in the experimental chamber of ARES. It consists out of nine thin gold wires at different angles to scan the projection of the transverse beam profile for different angles. The signal is detected with a beam loss monitor. After the measurement the tomography to reconstruct the beam sizes is performed using an algorithm developed at PSI and the beam parameters are determined from the resulting curve.

The goal of this report is to test the method by measuring the beam parameters of ARES with multiple quadrupole scans and to develop a tool to automate these measurements.

2 Theory

2.1 Beam dynamics

The design orbit of the particle beams is given as the trajectory of an ideal particle and is fixed by the layout of the accelerator. A particle bunch however contains many particles with different initial conditions. The trajectories inside the bunch therefore have a certain divergence in positions, angles and energy. In order to keep the particles inside the bunch close to their design orbit, it is necessary to repeatedly steer the diverging particles back onto their ideal trajectory. For this magnetic fields are used. The Lorentz force acts perpendicular to the path of the particles and changes their direction without further acceleration. The acting force $\vec{F}$ is given by

$$\vec{F} = q\,(\vec{E} + \vec{v} \times \vec{B}) \tag{1}$$

with q being the charge of the particle, $\vec{E}$ the accelerating field, $\vec{v}$ the velocity and $\vec{B}$ the magnetic field. Since we are looking at a case where the particle is not further accelerated and the magnetic fields are approximately perpendicular to the particle trajectory, Eq. 1 can be simplified to

$$F = q\,v\,B$$

The magnetic field close to the design orbit can be expanded as a sum of multipoles in a Taylor series. The multipoles have different effects on the particle path. To steer and focus the beam the dipole and quadrupole multipoles are used.

$$B_y(x) = \underbrace{B_{y0}}_{\text{dipole}} + \underbrace{\frac{\partial B_y}{\partial x}x}_{\text{quadrupole}} + \mathcal{O}(x^2)$$

The magnetic field can be normalized to the momentum to charge ratio q/p.

$$\frac{B_y(x)}{p/q} = \frac{1}{R} + kx + \mathcal{O}(x^2)$$

The dipole field bends the particle on a trajectory with the radius R. k is the quadrupole strength. Since the bending force resulting from the quadrupole field increases linearly with the transverse displacement from the ideal trajectory, the quadrupole field can be used to focus the beam. Since a quadrupole magnet consists of four poles, the magnet is focusing in one plane and defocusing in the other. To properly focus the beam, two quadrupoles with a relative rotation of 90°are needed. In dipole and quadrupole magnets the horizontal and vertical motion are decoupled and the motion in x- and in y-direction can therefore be treated independently. We will now analyse the beam dynamics in the x-s plane, s being the path length along the trajectory. Since the force is proportional to the displacement inside the quadrupole, the equation of motion for the particles resembles the harmonic accelerator. If we replace the time by the path length s as a free parameter, we obtain Hill's differential equation of motion

$$x''(s) - k(s)x(s) = 0.$$

For an accelerator the quadrupole strength k is not constant, but a function of the position s. The solution $x(s)$ of the differential equation is a quasi harmonic oscillation whose amplitude and phase depend on the position s along the trajectory.

$$x(s) = \sqrt{\varepsilon\beta(s)}\cos(\Psi(s) + \Phi)$$

ε and Φ are integration constants, $\Psi(s)$ is the phase advance. ε is called the emittance and is fixed by the initial conditions (e. g. the lase pulse shape, the laser spot size on the cathode and the cathode material). It stays constant for the whole length of the magnetic structure. The beta function $\beta(s)$ is determined by the focusing properties of the quadrupoles. Since the particles have varying initial conditions, the amplitudes $\sqrt{\varepsilon\beta(s)}$ of the trajectories form an envelope which defines the transverse beam size. In the case that the beta function $\beta(s)$ is known for the magnet structure the beam size can be estimated at any point s for a given beam emittance ε.

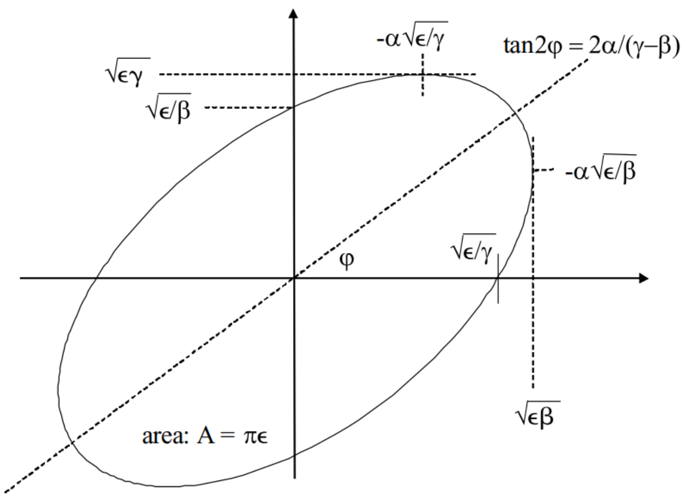

Figure 1: Phase space ellipse, taken from [2] (p. 158)

The emittance can also be interpreted in terms of the x-x'-phase space of the beam. For this we need to define the Courant-Snyder parameters (Twiss parameters) $\alpha(s)$, $\beta(s)$ and $\gamma(s)$.

$$\alpha(s) = -\frac{1}{2}\beta'(s) \qquad\qquad \gamma(s) = \frac{1+\alpha(s)^2}{\beta(s)}.$$

$\beta(s)$ is our beta function. The Courant-Snyder parameters allow us to compute the single particle trajectories between two locations without remembering the exact magnet structure. The particle trajectory coordinates at any given point fulfill the equation of an ellipse in the x-x'-phase space (Fig. 1):

$$\gamma(s)\, x^2(s) + 2\,\alpha(s)\, x(s)\, x'(s) + \beta(s)\, x'^{\,2}(s) = \varepsilon \tag{2}$$

The area of the ellipse is proportional to the emittance with $A = \pi\varepsilon$, the orientation and shape of the ellipse is described by the Courant-Snyder parameters. According to Liouville's theorem the area of the phase space ellipse and therefore the emittance ε are constants of the particle motions. Due to the different initial conditions of the particles inside the beam, each particle corresponds to an ellipse with a different area. Assuming the particle distribution to be of Gaussian shape, the average emittance is defined by the standard deviation σ of the particle distribution.

$$\sigma(s) = \sqrt{\varepsilon\beta(s)} \tag{3}$$

During the acceleration process, the emittance shrinks, but the normalized emittance $\varepsilon_n = \beta\gamma\varepsilon$ is conserved.

2.2 Measuring the beam emittance

The general equation of an ellipse is given by

$$\begin{pmatrix} x & x' \end{pmatrix} \mathbf{\Sigma} \begin{pmatrix} x \\ x' \end{pmatrix} = 1.$$

$\mathbf{\Sigma}$ is a real, symmetric, positive-definite matrix. For the phase space ellipse, $\mathbf{\Sigma}$ is called the beam matrix and describes the particle beam.

$$\mathbf{\Sigma} = \begin{pmatrix} m_{11} & m_{12} \\ m_{21} & m_{22} \end{pmatrix} = \begin{pmatrix} \langle x^2 \rangle & \langle x\, x' \rangle \\ \langle x\, x' \rangle & \langle x'^{\,2} \rangle \end{pmatrix} \tag{4}$$

The emittance can be calculated from the volume V:

$$\begin{aligned} V &= \pi\sqrt{\det \Sigma} = \pi\sqrt{m_{11}\, m_{22} - m_{12}^2} = \pi\, \varepsilon \\ \Rightarrow \varepsilon^2 &= m_{11}\, m_{22} - m_{12}^2 = \langle x^2 \rangle \langle x'^{\,2} \rangle - \langle x\, x' \rangle^2 \end{aligned} \tag{5}$$

Whilst Eq. 3 only holds under the assumption of Gaussian distribution, Eq. 5 is true for any particle distribution. Since the emittance from Eq. 5 is calculated from the beam size and the beam divergence, it cannot be measured directly. By measuring the beamsize with varying quadrupole strengths ("quad scan") or at different positions ("z-scan"), we can manipulate the Twiss parameters and therefore the orientation and shape of the phase space ellipse in order to determine the beam emittance. Both methods are equivalent, but in practice varying the quadrupole strength is easier than varying the measuring position.

Comparing Eq. 2 and Eq. 4, we can define $\mathbf{\Sigma}$ as

$$\mathbf{\Sigma} = \begin{pmatrix} m_{11} & m_{12} \\ m_{21} & m_{22} \end{pmatrix} = \varepsilon \begin{pmatrix} \beta & -\alpha \\ -\alpha & \gamma \end{pmatrix}. \tag{6}$$

The transformation of a particle trajectory from a starting point s_0 to any other point s can be described by

$$\begin{pmatrix} x \\ x' \end{pmatrix} = \begin{pmatrix} C & S \\ C' & S' \end{pmatrix} \begin{pmatrix} x_0 \\ x'_0 \end{pmatrix}. \tag{7}$$

C, S, C' and S' are the elements of the transformation matrix. If we solve Eq. 7 for x_0 and x'_0 and insert the result into the phase space ellipse equation, Eq. 2, we get the equation

$$\begin{aligned} \varepsilon = {} & \underbrace{(C'^2\beta_0 - 2S'C'\alpha_0 + S'^2\gamma_0)}_{\gamma}\, x^2 \\ & + 2\,\underbrace{(-CC'\beta_0 + S'C\alpha_0 + SC'\alpha_0 - SS'\gamma_0)}_{\alpha}\, xx' \\ & + \underbrace{(C^2\beta_0 - 2SC\alpha_0 + S^2\gamma_0)}_{\beta}\, x'^2. \end{aligned} \tag{8}$$

Comparing Eq. 8 to Eq. 2, the transformation properties of the Courant-Snyder parameters can be determined. Using Eq. 4 and 6, the beam size σ after the transformation can be determined by

$$\sigma^2 = \langle x^2 \rangle = \varepsilon\beta = C^2 m_{0,11} + 2CS m_{0,12} + S^2 m_{0,22}. \tag{9}$$

If we now measure the beamsize σ for different quadrupole strengths k, we can fit the matrix elements of the initial beam matrix and determine the emittance with Eq. 5. To achieve a good fit, it is important to vary the quadrupole strength, so that the narrow focal point of the quadrupole is included in the scan. The parameters S and C of the transformation matrix can be calculated through beam optics. The quadrupole can be treated as a thin lense if its length l_q is much smaller than the distance d to the measuring point, $l_q \ll d$. The focal length f of a quadrupole is calculated via

$$f = \frac{1}{k\, l_q}. \tag{10}$$

The transform matrix can then be calculated as

$$\underbrace{\begin{pmatrix} 1 & d \\ 0 & 1 \end{pmatrix}}_{\text{drift}} \underbrace{\begin{pmatrix} 1 & 0 \\ -\frac{1}{f} & 1 \end{pmatrix}}_{\text{focusing}} = \begin{pmatrix} 1 - \frac{d}{f} & d \\ -\frac{1}{f} & 1 \end{pmatrix}. \tag{11}$$

Using Eq. 9 and inserting Eq. 10 and 11, we get the equation to fit the data:

$$\begin{aligned} \sigma^2(k) &= (1 + dkl_q)^2 m_{0,11} + 2(1 + dl_q k) d m_{0,12} + d^2 m_{0,22} \\ \Rightarrow \sigma^2(k) &= (d^2 l_q^2 m_{0,11}) k^2 + 2(dl_q m_{0,11} + d^2 l_q m_{0,12}) k \\ &\quad + (m_{0,11} + 2d m_{0,12} + d^2 m_{0,22}) \end{aligned} \tag{12}$$

Eq. 12 can be fitted with a parabola of the form $Ak^2 + Bk + C$. From the coefficients of the fit, we can determine the matrix elements of the beam matrix via

$$\begin{aligned} m_{11} &= \frac{A}{d^2 l_q^2} \\ m_{12} &= \frac{B - 2dl_q m_{11}}{2d^2 l_q} \\ m_{22} &= \frac{C - m_{11} - 2d m_{12}}{d^2} \end{aligned}$$

With the elements of the beam matrix we can calculate the emittance and the Courant-Snyder parameters using Eq. 5 and 6. [1, 2]

3 Experimental set up

3.1 ARES

The measurements were performed at the **ARES** accelerator (**A**ccelerator **R**esearch **E**xperiment at **S**INBAD). ARES is a normal conducting radio-frequency electron linear

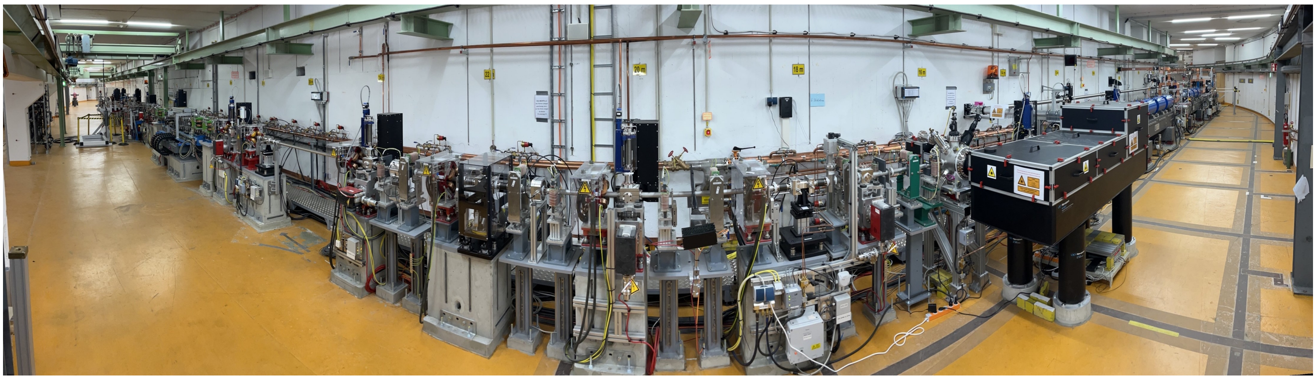

Figure 2: ARES set-up

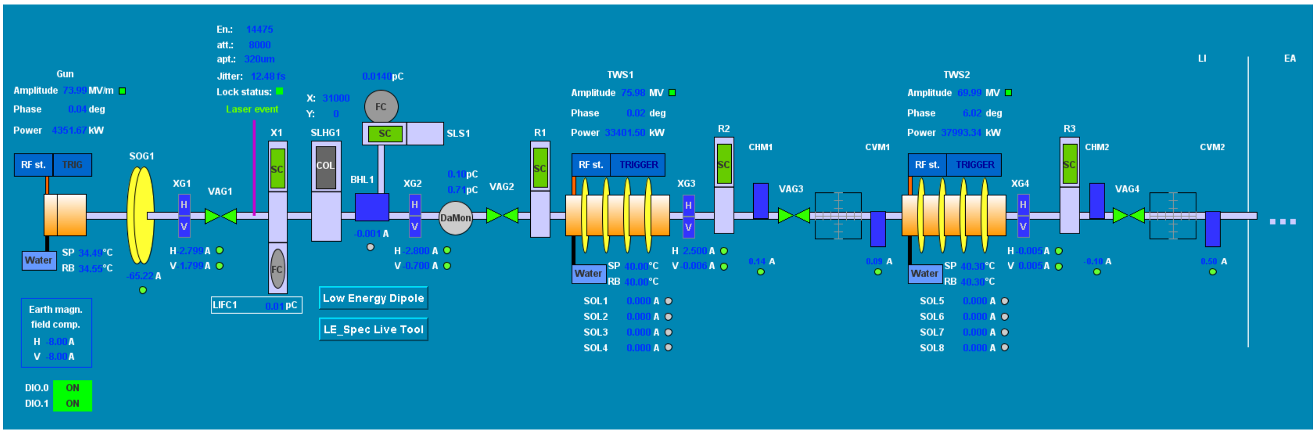

Figure 3: Linac section

accelerator at the R&D facility SINBAD (**S**hort **IN**novative **B**unches and **A**ccelerators at **D**ESY) in the former DORIS accelerator tunnel at DESY with a target energy of 50-155 MeV that is currently in its commissioning phase. Its goal is to provide low charge, short electron probe bunches with excellent arrival-time stability in the (sub-)fs regime.

The electrons for the accelerator are generated in the gun section by a normal conducting RF photoinjector. This photoinjector consists of an interchangeable photocathode where the electrons are produced via the photoelectric effect using a drive laser from the laser laboratory outside the tunnel. The electrons are accelerated immediately to 3.4 MeV inside the RF gun cavity. At the moment the electron bunches are produced with a 10 Hz repetition rate. After the gun section the electron beam is focused by a dual-coil solenoid magnet in both transverse directions, followed by a diagnostic sections.

The acceleration is achieved in the Linac section (Fig. 3). Two traveling wave copper structures operating at a frequency of 2.998 GHz accelerate the electrons to their target energy. In the on-crest mode the electrons reach an energy of 155 MeV.

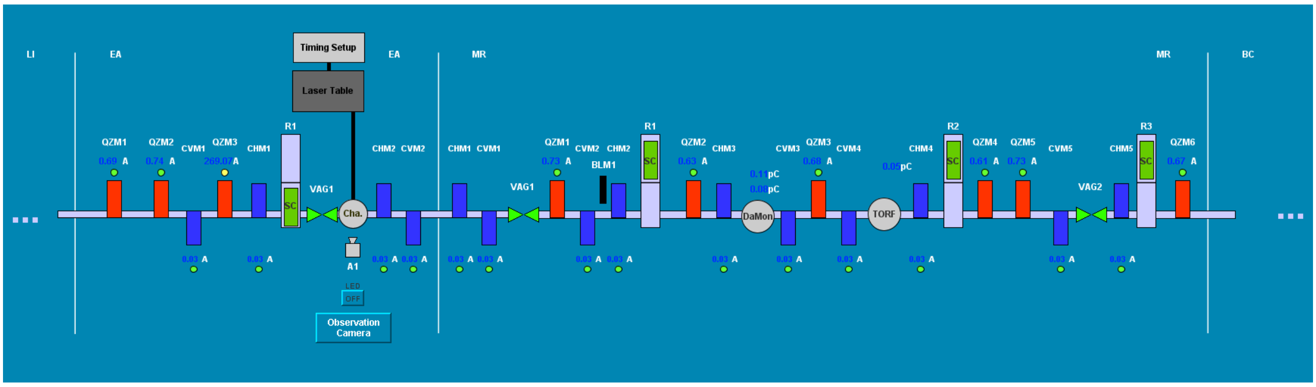

Figure 4: Experimental area and matching region

The experimental area used in the measurements is situated between the second traveling wave structure and the matching region (Fig. 4). It consists of three quadrupole magnets (QZM1, QZM2 and QZM3) that form a final focus triplet to achieve beamsizes in the order of a few micron, a screen station with a camera for beam profile diagnostics and the experimental chamber. A set of dipole magnets is situated at the end of the Linac section for vertical and horizontal beam steering through the quadrupoles. Another set of magnets is located in front of the experimental chamber to steer the beam onto the experiments inside the experimental chamber. One of the dipole magnets can be found between QZM2 and QZM3, the other downstream of QZM3. The experimental chamber contains a high-precision hexapod positioning system which can move with six degrees of freedom. The precision of the hexapod is 1 nm in x-y-z direction and 1 µrad in θ_x-θ_y-θ_z direction. The experiments can be mounted on a target platform on top of the hexapod. For the wire scan measurements, a scintillating Yttrium Aluminium Garnet crystal (YAG screen) and a wire scanner are fastened on the platform. Two cameras are installed on top of the experimental chamber, one focused on the YAG screen to see the beam profile and on focused on the whole platform to observe the hexapod.

Downstream of the experimental chamber in the matching region a beam loss monitor detects electromagnetic showers outside of the beam pipe by scintillation. The signal is proportional to the loss.

The accelerator is operated via a control system based on DOOCS (**D**istributed **O**bject-**O**riented **C**ontrol **S**ystem). [3, 4]

3.2 Wire scanner

A wire scanner can be used for transversal beam profile measurements. A very thin wire is moved through the beam and generates losses by the formation of an electromagnetic shower through the interaction of the beam with the wire. These losses can escape the

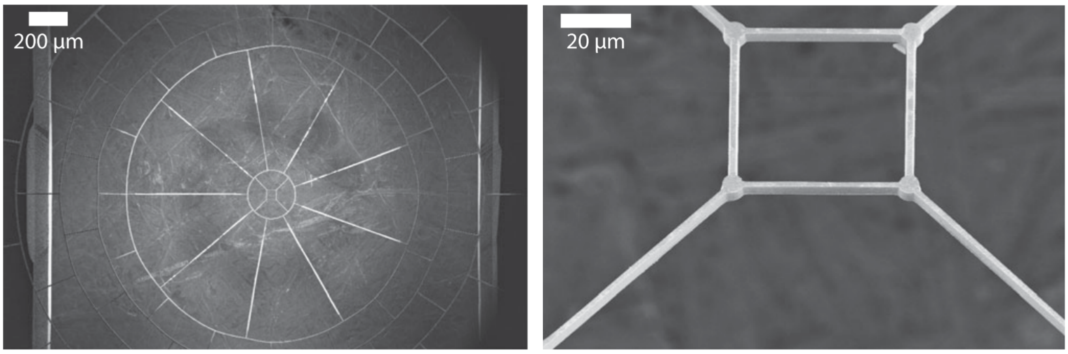

Figure 5: Scanning electron microscope images of the free-standing wire scanner device, taken from [6]

beam pipe and are partially detected outside of it by a scintillating beam loss monitor. The signal of the scintillator is proportional to the losses and therefore to the beam intensity at the position of the wire. The one-dimensional beam profile in direction of the wire movement can then be reconstructed from the signal at the different wire positions and the transverse beam size can be estimated. The advantage of wire scanners is that they have a high spatial resolution whilst being minimal invasive to the beam operation. It is not a single-shot method, but needs multiple shots from the electron gun to probe the beam size. The geometric resolution of a wire scanner is inversely proportional to the width. A conventional screen-based method can give us the two-dimensional profile at one shot, but is destructive to the beam and has a worse resolution. The wire scanner can achieve submicron resolution whilst the screen-based method is limited to a few microns.

The wire scanner used in the experiment was fabricated at the Paul-Scherrer-Institute (PSI) in Switzerland using nanotechnology with electron beam lithography to achieve a submicron resolution. It consists of nine homogeneously-spaced free-standing radial gold wires at different angles which are supported by a spiderweb-shaped structure attached to a silicon frame. The wires have a width of 1 µm. At the center of the structure a square is located that can be used for centering the beam on the wire scanner. The hexapod moves the wire scanner through the beam on a polygon path so that each of the wires transverses the beam orthogonally. This allows us to measure nine different projections of the transverse beam profile.[5, 6]

3.3 Tomography

With the nine projections of the transverse beam profile we can reconstruct the transverse beam profile using a tomography method developed at PSI. The reconstruction algorithm is base on a macroparticle distribution which uses less particles for the beam, but with a higher charge for each. The total particle density is given by constructing a Gaussian distribution around each macroparticle. Starting from a homogeneous distribution, the distribution of macroparticles is iteratively optimized to match the measured projections. The tomography algorithm can reconstruct arbitrary transverse profiles of the electron beam. However, the algorithm includes a random number, so that each reconstruction differs slightly from the previous one. This also leads to a variation in the calculated beam parameters for different reconstructions of the same data.[6]

3.4 Performing the scans

The measurements were first performed using a Python script and later with the implemented wire scanner tool. Before each wire scan the beam has to be aligned centrally on the YAG screen. Since the position distance between the YAG screen and the wire scanner is known, this corresponds to a good central alignment on the wire scanner. A polygon path for the hexapod is then calculated and the hexapod moves the wire scanner on this path to detect the projections of the beam profile. For each wire position the average signal and the standard deviation for a given number of different shots from the electron gun are recorded for the beam loss monitor. Several other figures of merit are saved alongside the beam loss signal.

The quadrupole scan performs multiple wire scans for varying strengthes of a chosen quadrupole. For this a good symmetrical alignment inside the quadrupoles is necessary. If the alignment of the beam is asymmetrical inside the quadrupoles a change in the quadrupole strength leads to a change of the beam position inside the experimental chamber. The beam is the no longer centered on the wire scanner which can greatly effect our results. Though one can also correct for this effect by steering the beam with the dipoles back to its optimal position, a good symmetrical alignment from the start has proven to by the more effective method. This can be achieved by steering the beam with the two dipoles at the end of the Linac section until no change in position is observed when changing the quadrupole strength. To keep the good alignment during the scan, it is important to cycle the quadrupole and recheck the alignment. The quadrupole should then be cycled again before the scan. In addition, the range of the scanned quadrupole strengths should be chosen so that the beam is not too large at the minimum and maximum and that the focus point of the quadrupole is somewhere in the middle.

The analysis was performed with the Python script or later with the wire scanner tool.

4 Measurement results

All measurement were performed for a beam charge of approximately 0.2 pC.

4.1 Single wire scan

In the beginning, single wire scans were performed to get accustomed with the measuring process and the reconstruction. The measurements were performed as described in section 3.4. In cases where some of the signal peaks were partly cut away at the edge of the scan range for the wire, the reconstruction could still be performed though with a much worse convergence. Since the alignment of the beam on the wire scanner does not have to be perfectly central, the quad scan can be performed for a large number of scan points even if the beam shifts a bit. For each single wire scan a visualisation of the signal is plotted (Fig. 6).

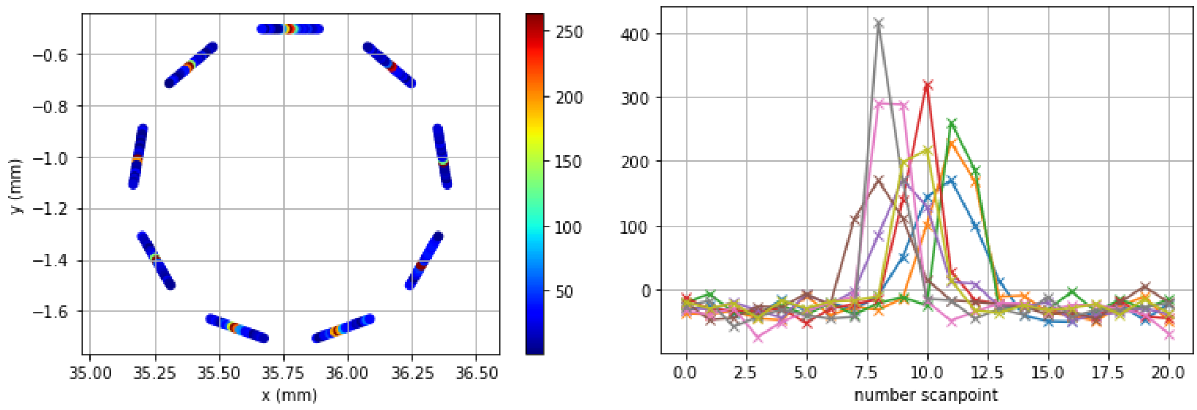

Figure 6: Signal of a very well aligned single wire scan; left: signal marked on the polygon path; right: the signal for all wires together

The results of the reconstruction can be seen in Fig. 7 and 8. The tomography reconstructs the whole two dimensional beam profile, as can be seen in Fig. 7. In order to compare the reconstructed beam profile to the measured data points, the reconstruction is projected onto the wire angles. If a reconstruction was possible, the projections and the measured data agree quite well in general. The calculation of the beam sizes is visualised in Fig. 8. The beam profile is projected onto the x- and y-direction and fitted with a Gaussian. Two common problems seen in the tomography are that either artefacts can appear at the side of the beam reconstruction or a part of the normal small background is totally cut away. This is most commonly seen in reconstruction of scans with a very bad alignment where some peaks are already partly cut away at the edge of the scan region or where the beginning peak of another wire can already be seen. This has an impact on our fitted Gaussian beam sizes since the whole range is fitted, especially in the case of large artefacts. In addition, it can be seen that the beam profile can be quite asymmetric and therefore not ideal to approximate with a Gaussian. Nevertheless, the fit has proven to bring overall good results.

To investigate the stability of the wire scan, a single wire scan was repeatedly performed for the same accelerator settings for an extended period of time. The beam was focused in y-direction. This was done first without a reference phase correction for the second traveling wave structure (TWS2) and later with the phase correction (Fig. 9 and 10). The reference phase correction ensures that the phase of the input signal for TWS2 stays constant by comparing it to a reference phase. In Fig. 9 it seems as though a small

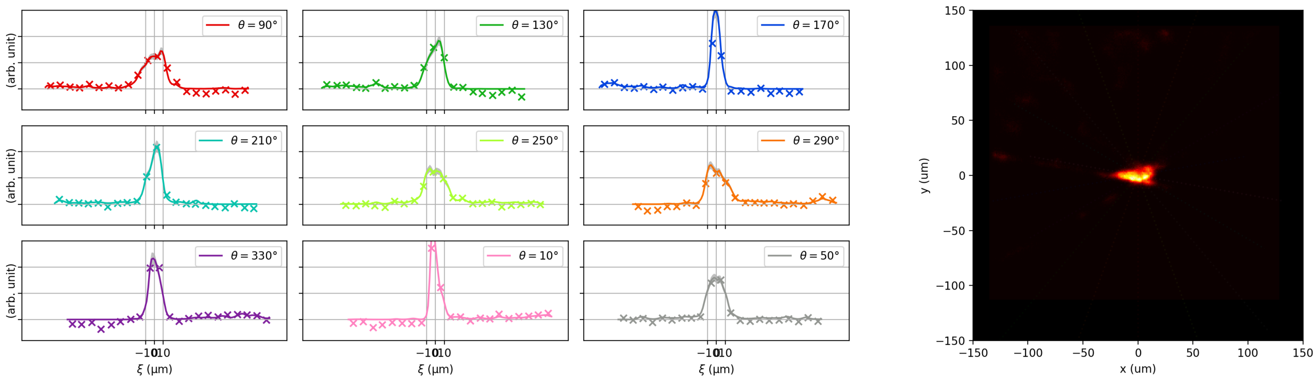

Figure 7: Tomography of a single wire scan

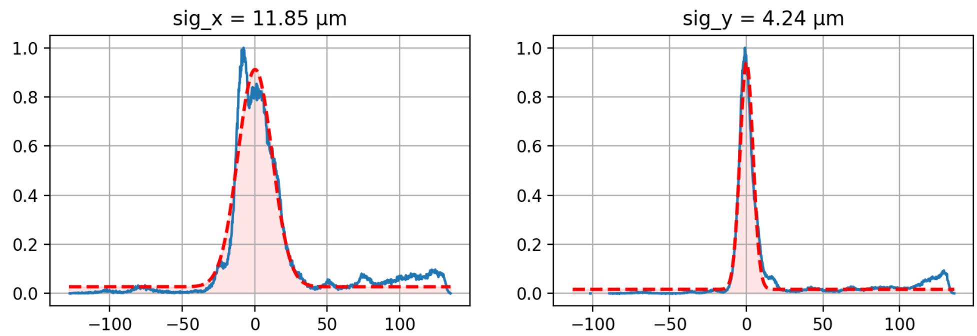

Figure 8: Calculated beam sizes from a single wire scan

drift can be observed. The beam sizes vary over a range of 2.5 micron in x-direction and 1.8 micron in y-direction over the course of 1.5 hours. The maximum variation between the measurements is 1 micron. Contrary to expectation, the variation of the beam sizes with the TWS2 phase correction seems larger (Fig. 10). The beam size in x-direction varies over a range of 2.5 micron with a maximal variation of 2.1 micron between the measurements. The beam size in y-direction is relatively stable.

4.2 Quadrupole scan

The quadrupole scans, were carried out as described in section 3.4. In the first quadrupole scans steerer settings were noted down for each scan point to keep the beam on the wire scanner. In all following measurements the scan was performed with a good symmetrical alignment. After the first few measurements it was also made sure off that the magnet was cycled before the measurement and that the alignment on the screen was still good after the magnet was cycled. The first six scans were done with the QZM3 quadrupole. Further nine measurements were performed with the QZM2 quadrupole. The adventage of QZM2 is that the two dipole magnets that are used to align the beam on the screen are both behind the quadrupole. The fringe fields of the magnet affact eachother. The

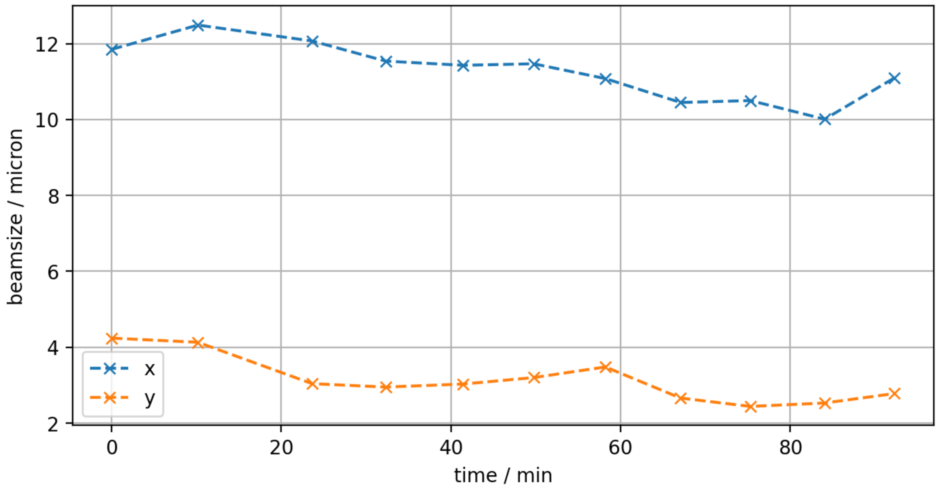

Figure 9: Stability measurement of the beam size without reference phase correction for the second traveling wave structure (TWS2)

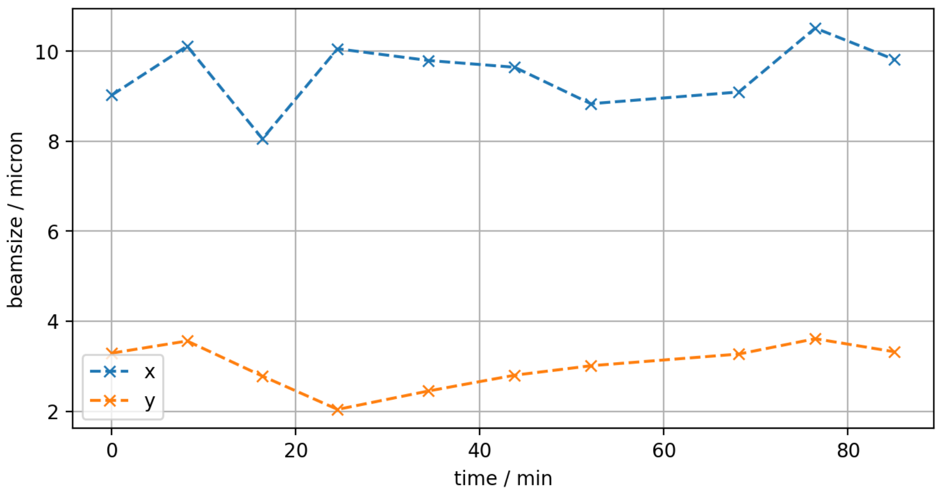

Figure 10: Stability measurement of the beam size with reference phase correction for the second traveling wave structure (TWS2)

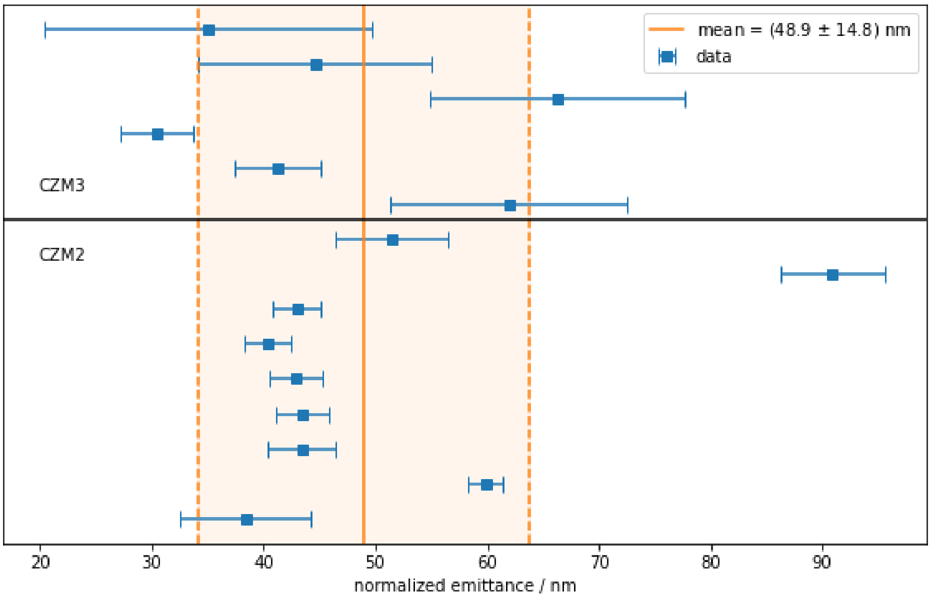

Figure 11: Normalized emittance ε_n of the quad scans

idea is therefore that the handling of QZM2 is easier. On the other hand QZM3 should be able to achieve a tighter focus since it is closer to the experimental chamber. Scans for both magnets were performed in x- and in y-direction. In Fig. 11 and 12 the normalised emittance ε_n of all quad scans is presented . In Fig. 13, 14 and 15 the results for the Twiss parameters are plotted separately for the x- and y-direction. The averages of the estimated parameters can be found in Table 1.

parameter	value
ε_n	(48.9 ± 14.8) nm
ε_n (QZM2)	(46.6 ± 13.2) nm
ε_n (QZM3)	(50.4 ± 15.6) nm
α (x-direction)	(170.7 ± 23.3)
α (y-direction)	(-45.3 ± 10.6)
β (x-direction)	(108.1 ± 14.6) m
β (y-direction)	(64.5 ± 18.6) m
γ (x-direction)	(269.7 ± 9.1) m^{-1}
γ (y-direction)	(32.8 ± 9.1) m^{-1}

Table 1: Results of the quad scans

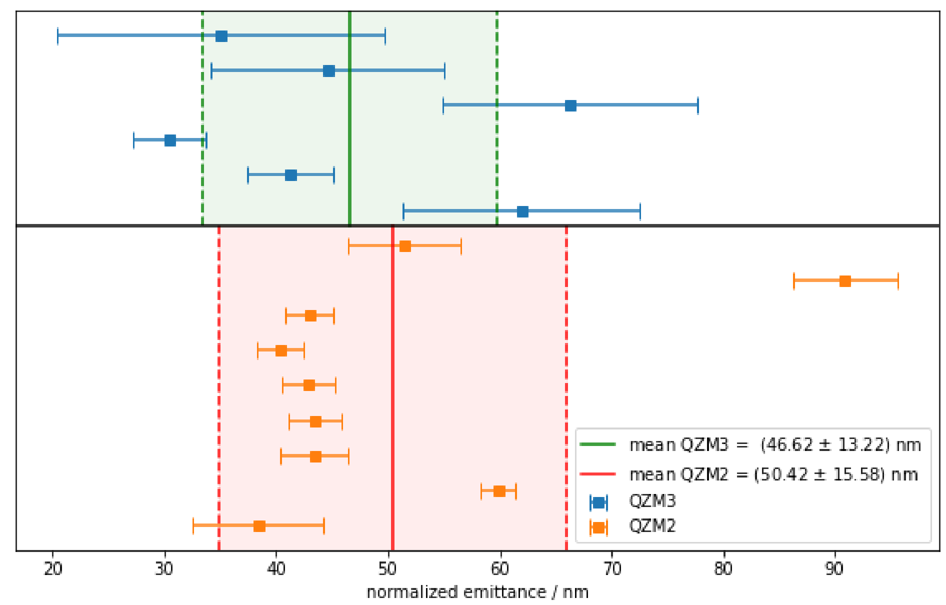

Figure 12: Normalized emittance ε_n of the quad scans, seperated in QZM2 and QZM3

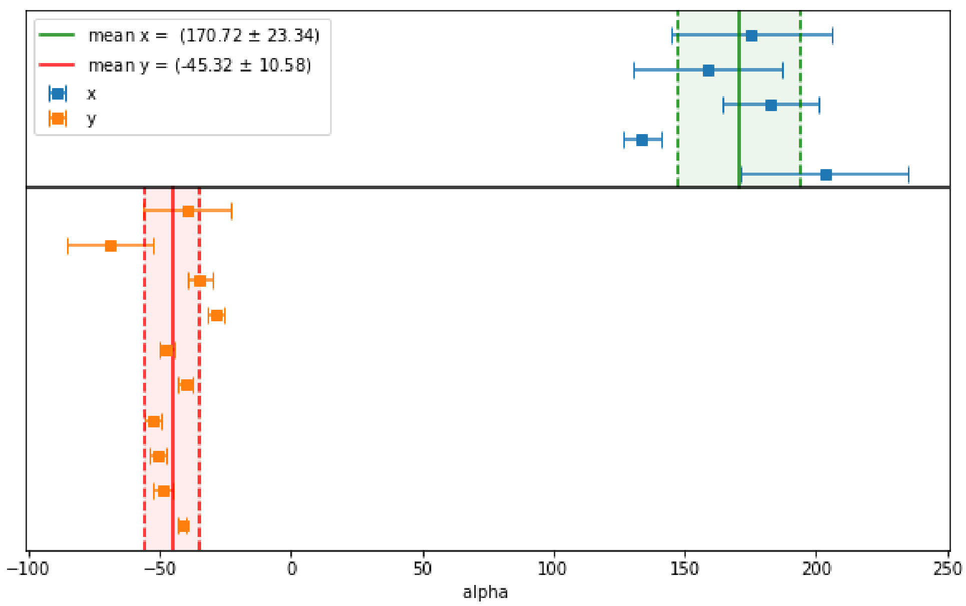

Figure 13: Twiss parameter α of the quad scans, seperated in x- and in y-direction

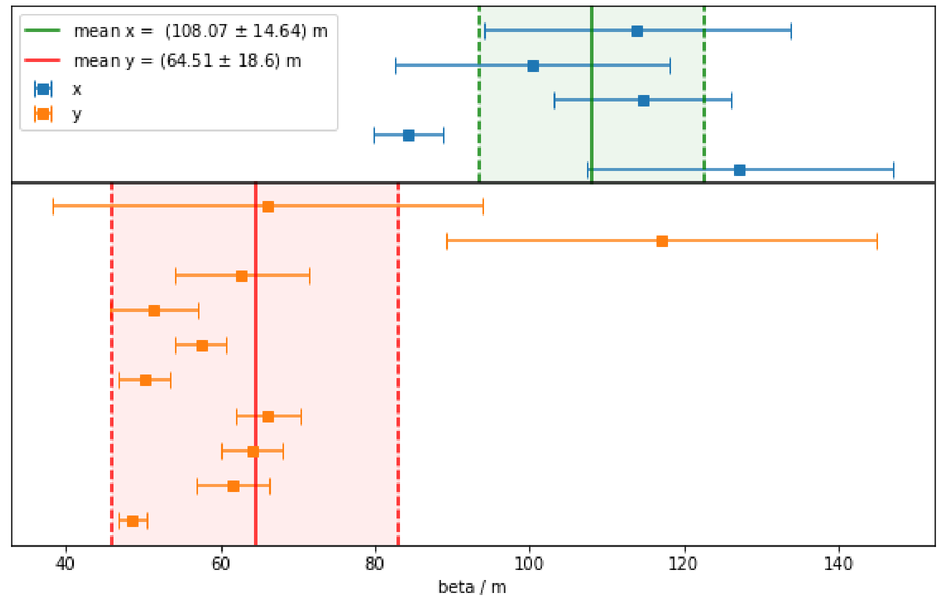

Figure 14: Twiss parameter β of the quad scans, seperated in x- and in y-direction

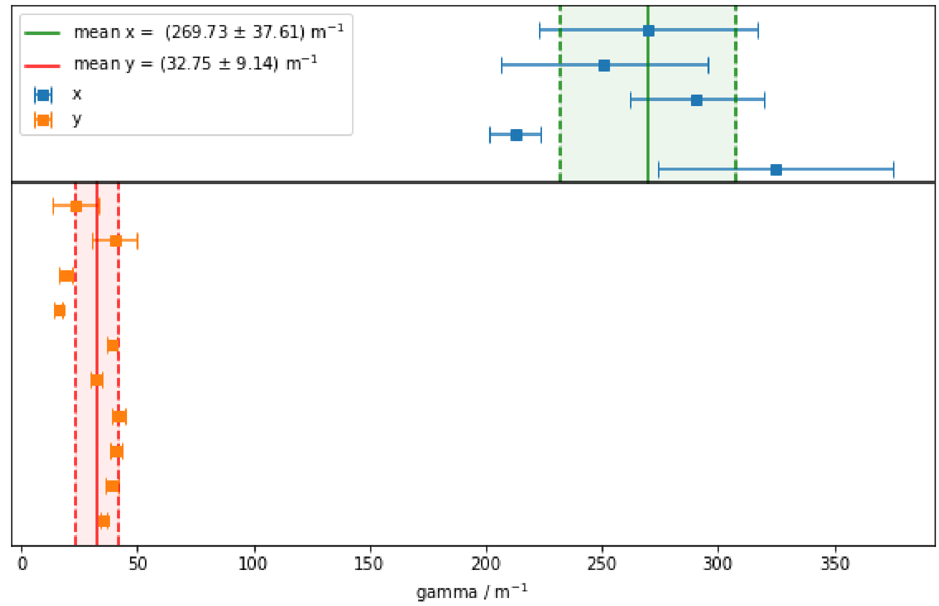

Figure 15: Twiss parameter γ of the quad scans, seperated in x- and in y-direction

5 Implementation of the wire scanner tool

5.1 Introduction to the wire scanner

There are already different tools implemented on the ARES control panel e. g. to load machine state files. In order to make the wire scanner more efficient and user-friendly, I implemented a tool that can be controlled via a GUI for the scan (Fig. 16). The tool will later be accessable via a button on the controll panel. With the tool a single wire scan, a test whether the alignment of the wire scanner is good and a quad scan can be performed. It includes the measurement and the full analysis. The scan signal is dynamically visualised in a plot window, as are the plots from the analysis.

The wire scanner tool was implemented via Python. For the GUI the Python package *Qt5* was used. The communication to the accelerator was done with *pydoocs*, the Python version of DOOCS.

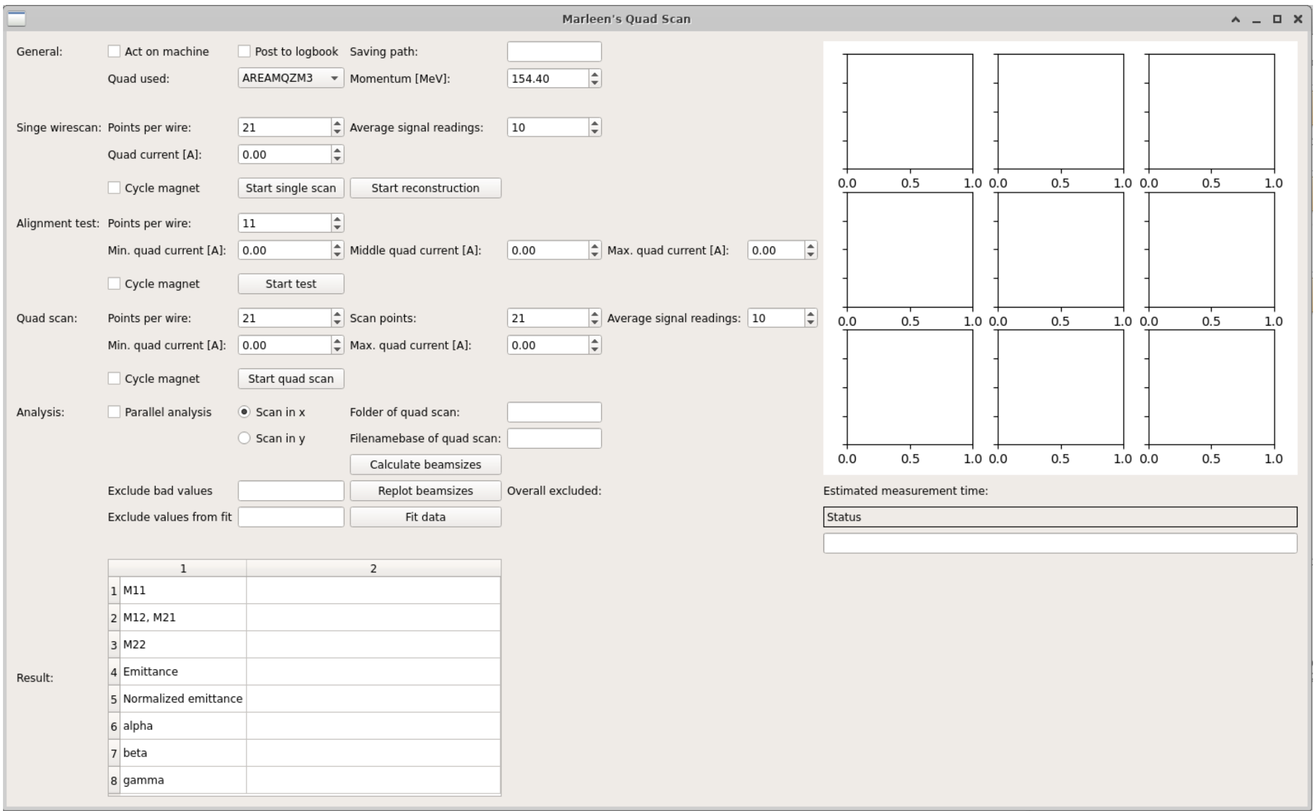

Figure 16: GUI of the wire scanner tool

5.2 General

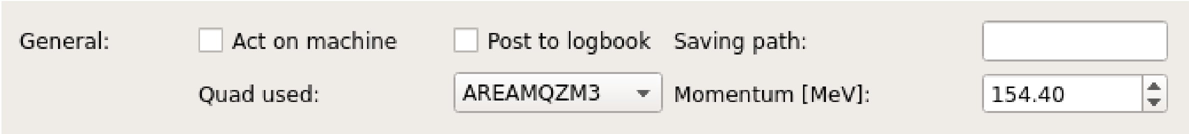

Figure 17: General section of the wire scanner tool

In the General section parameters that are important for all the scans can be entered (Fig. 17). The tool can only change parameters in the accelerator system if *Act on machine* is checked. If a measurement is started without it being checked, an error is raised in the status bar. If *Post to logbook* is checked, the tool can forward information to the logbook. For the single wire scan, the alignment test and the quad scan a message is printed to the logbook with the elapsed time and the filename when the scan is finished. For the fit of the quad scan the values of the resulting beam parameters are printed to the logbook. In addition, a saving path can be entered. If a path is chosen, the measurement will be saved under this path. If no no path is entered, a folder with the current data is created under which all the measurements of the day are saved. Each measurement has its own folder which is named after the type of measurement, the used quad, the data and the start time. The quadrupole can be selected under *Quad used*. The momentum is entered and broadcasted to the accelerator in order to get the correct values from the quadrupole strengths.

In the plotting window the results for the analysis are plotted (Fig. 18), i. e. the tomography of the single wires scan, the calculated beam sizes for the quad scan and their fit for the beam parameters. In addition, during the measurements the measured signal for the wires is plotted dynamically. A subplot is created for each wire. The estimated measurement time for each measurement is printed underneath the plot. Since the averaging over a different number of gun shots was not tested enough, it only estimates the time as if the average over ten images was taken. This can nevertheless be easily adjusted in the code once further measurements were done. In the status bar the current process step of the wire scan tool is printed. If an error is raised, this is printed too. Underneath the status bar the progress bar shows the current advance of the scan.

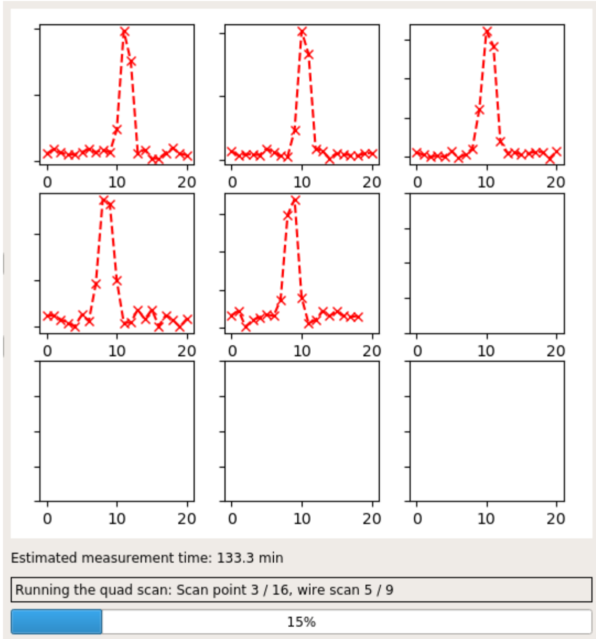

Figure 18: Plotting window, status and progress bar of the wire scanner tool

5.3 Measurement

5.3.1 Single wire scan

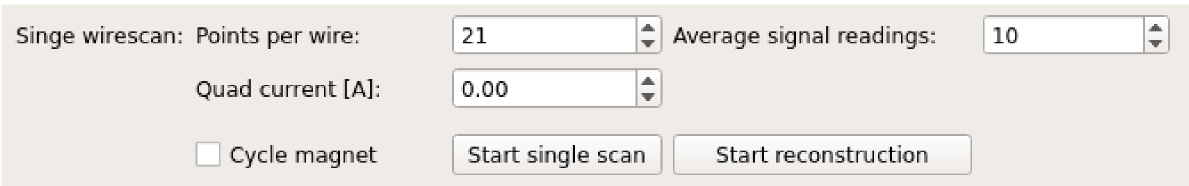

Figure 19: Single wire scan section of the wire scanner tool

The single wire scan can perform the full wire scan and beam profile reconstruction for one set quadrupole current (Fig. 19). For the single wire scan the number of points that should be scanned per wire can be entered. For a good measurement a minimum of 21 points is advisable. For a quick measurement 11 are sufficient. The scan range of the polygon path stays the same. The number of signals of the beam loss monitor over which is averaged to get the final value, can also be adjusted. For each reading of the beam loss signal, the machine waits for a new macropulse (another shot from the electron gun), so that it really takes different data points to calculate the average. All measurements in this report were done by averaging over ten signals. The current of the chosen quadrupole can also be set for the single wire measurement. If no quadrupole current is set, i. e. the entered value stays at 0.00, the current is not set, but stays the same as specified in the machine. If the current is set, the machine waits for it to be stable enough around the set value to continue. In the case that *Cycle magnet* is checked, the chosen quadrupole is cycled before the measurement. Otherwise it might happen, that the currents have an offset due to the hysteresis curve and the focus point is no more located in the middle of the scan range.

The measurement is started with *Start single scan*. It checks if it can act on the machine, created a folder and then sets the momentum of the beam. If checked, the magnets are cycled and then the currents are set. The hexapod is moved to its center position and the wire scan along the polygon path is started. The hexapod moves to every point on the polygon path, waits if the machine state is clear and if everything is fine, it reads out the values, takes as many values as it should average over from different macropulses and takes their mean and standard deviation for the final loss signal. The data is then written to the file of the specific wire and the signal point is added in the plot window. In the end, a colorplot of the signal on the polygon path and a plot of all the wire signals together are saved in the same folder (Fig. 6).

With *Start reconstruction* the tomography can be performed. If a wire scan was just performed, the path of the wire scan is temporarily saved and the tomography will be performed on these files. Otherwise, it will be checked whether a path was given in *Saving path* to perform the tomography on older data. The tomography uses the algorithm developed at PSI. In one figure the reconstructed transverse beam profile and the projections of the reconstructed beam for all nine wires alongside the measured signal are plotted (Fig. 7). In another figure the projection of the reconstructed beam profile in x- and y-direction together with a fitted Gaussian and the σ beam size of the Gaussian are plotted (Fig. 8). The σ value is taken as the geometric beam size.

5.3.2 Test alignment

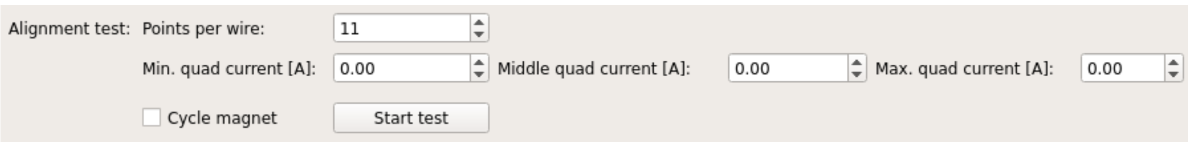

Figure 20: Test alignment section of the wire scanner tool

The alignment test is used to check whether the beam is really centered on the wire scanner. It is similar to the single wire scan (Fig. 20). Instead of scanning all the wires, only the first and the third wire are scanned, since they are almost horizontal and vertical. If the beam is well centered in these both direction, it will also be well centered for all the other wires. To check the alignment 11 points per wire and 10 points for averaging are enough though the points per wire can be adjusted. The beam is scanned for three different currents. These should be the minimal, the middle and the maximal currents that are later used in the quadrupole scan. Before the alignment test, the quadrupole should be cycled. Starting with the middle current, the first and third wire are scanned for all three currents. For each current the machine waits until it is stable close to the set point. The signal is again dynamically plotted in the plotting window, so that one can see the alignment.

5.3.3 Quad scan

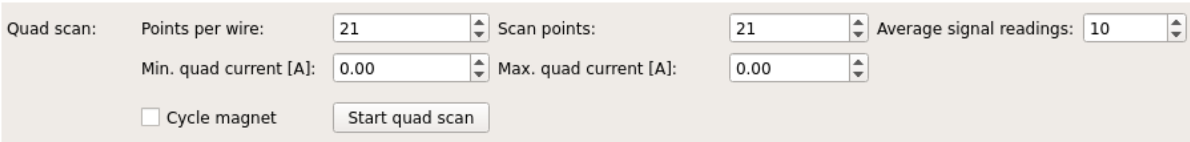

Figure 21: Quad scan section of the wire scanner tool

The quad scan takes the data we need to calculate the emittance and the Twiss parameters of the accelerator (Fig. 21). Before the quad scan it is very useful to do the alignment test. The quadrupole should also be cycled to ensure that the focus of the quadrupole stays in the middle. *Scan points* determines for how many quadrupole settings a wire scan is performed. For a good fit at least 21 should be scanned. The scan points are equally distributed between the minimal and the maximal current. The number of signals to average over for the final beam loss value. If the quad scan is started, it performs a single wire scan at each of the scan points. Again, the machine waits for stability after setting each current. If *Post to logbook* is checked, a message is posted to the logbook after each single wire scan that includes the elapsed time and in the filename base of the wire scan. In the filename base the current index of the scan point is included. After all wire scans are finished, a message is posted to the logbook that the quadrupole scan is finished together with the total elapsed time. The folder and filename base of the quad scan is saved in a label for the following analysis.

5.4 Analysis

In the analysis the data from the quad scan is fitted and the beam parameters are calculated (Fig. 22). The beam sizes for the quadrupole scan are calculated by performing the tomography for each scan point and taking the σ beam sizes in x- and y-direction from the Gaussian fit to the projection in these two directions. If *Parallel analysis* is checked, this is done in parallel by using the *threading* package in python. The setting is advisable since it is much faster. The two boxes *Scan in x* and *Scan in y* are important for the fit. The fit has to know in which direction the beam was focused to fit exactly these measured points. If a folder and a filename are entered in the corresponding fields, the measured data will be taken from these places. Otherwise it will be checked, whether the folder and the filename base from a previous quad scan are saved in a label next to these boxes to perform the analysis on. *Calculate beamsize* starts the analysis of the measured quad scan data. The beam sizes are calculated with the PSI tomography method in parallel or not depending on whether *Parallel analysis* is checked. The calculated beamsizes together with the quadrupole stengths of the scan points are saved in a

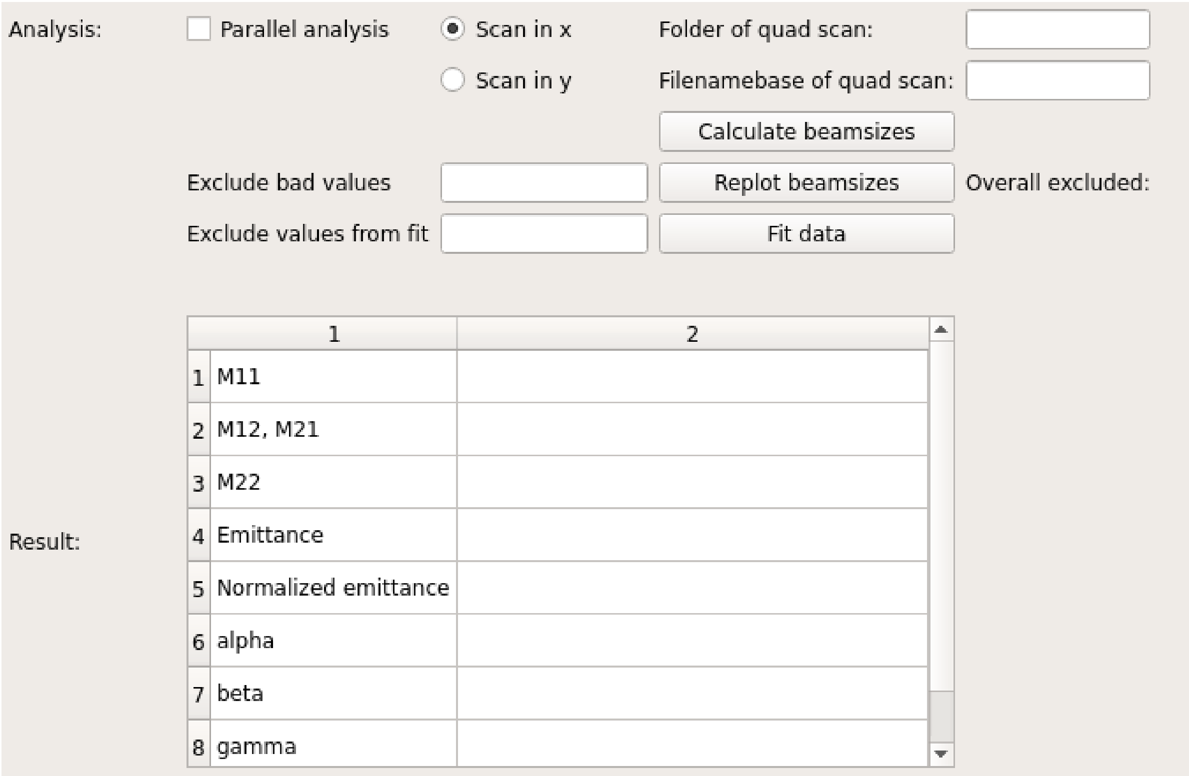

Figure 22: Analysis section of the wire scanner tool

result *.txt*-file inside the folder of the quad scan. To calculate the beam sizes the filename base of the measured data has to be also entered. After the calculation is finished, the beam sizes in x- and y-direction are plotted versus the quadrupole strength. The plot is shown in the plotting window and saved as a *.png*-image.

For the replot and the fit the folder name is enough since both methods take their input from the result *.txt*-file. Eventhough the measurement waits for the machine state, other things can also go wrong and might render a wire scan for a certain scan point unusable. In this case, the indeces of these scan points seperated by commas can be entered into *Exclude bad values*. With *Replot beamsize* the picture of the beamsize versus the quadrupole strength from the analysis is replotted without the bad value and again saved as a *.png*-image. The excluded values are then temporarily saved under the label of *Overall excluded*. For the fit more points can be specificly excluded by entering them under *Exclude values from fit* in the same way. The overall excluded points from before will be excluded in addition. With *Fit data* the fit is performed. A parabola is fitted to the data points that were not excluded. From the fit the parameters of the parabola and there covariance matrix can be determined. From these the beam parameters can be calculated with Eq. 12, 5 and 6. For the matrix elements of the beam matrix, the emittance and the normalized emittance the standard deviation is determined by taking into acount the full correlation between the parameters of the parabola. Since the formula for the emittance is non-linear, there is no analytical formula to take the correlation into account for the Twiss parameters. The standard deviation in this case is calculated by assuming the matrix elements and the emittance to be uncorrelated. Otherwise the standard diviation would have to be determined via Monte Carlo methods. The calculated parameters are entered into the result table and saved as a *.txt* file under the folder of the quadrupole scan. The fit is plotted inside the plotting window and saved as a *.png*-image. The points that were used for the fit are plotted in orange and the points that were not used in blue. Points where the accelerate did not match the set values, e. g. due to vacuum events, are excluded overall and not plotted. The fitted parabola is plotted in green.

6 Summary and Outlook

We showed that the emittance measurements with the quadrupole scan works and improved the method to produce the best results. The normalized emittance was determined to be in the region of 35 to 65 nm. The values for the quadrupoles QZM2 and QZM3 seem to lie in the same regime.

The emittance was also determined by performing ASTRA simulations. ASTRA is a space charge tracking algorithm that can be used to simulate the accelerator and from this calculate different parameters. The ARES accelerator and the quadrupole scan were simulated inside ASTRA and the beam emittance was determined to be 80 to 90 nm. This is a lot higher than the measured value. In order to determine where this difference might stem from further simulations have to be performed. Since the initial conditions are not perfectly known, it is possible that the difference might arise from this issue.

The wire scan tool was also implemented successfully and tested in its operation. It runs without any problems and will be used to determine the emittance and the other beam parameters in future experiments. It will also be used as a tool to calibrate the screen-based methods used at ARES.

References

[1] Klaus Wille, *The Physics of Particle Accelerators. An Introduction*, pp. 44-83, Oxford University Press, 2000.

[2] Helmut Wiedemann, *Particle Accelerator Physics*, pp. 158-166, Springer-Verlag Berlin Heidelberg New York, 2007.

[3] Eva Panofski et al., *Commissioning Results and Electron Beam Characterization with the S-Band Photoinjector at SINBAD-ARES*, Instruments 2021, 5, 28, DOI: 10.3390/instruments5030028, 2021.

[4] Florian Burkart et al., *The Experimental Area at the ARES Linac*, DOI: 10.18429/JACoW-IPAC2019-MOPTS014, 2019.

[5] G. L. Orlandi et al., *Nanofabricated free-standing wire scanners for beam diagnostics with submicrometer resolution*, Physical Review Accelerators and Beams, Vol. 23, 042802, DOI: 10.1103/PhysRevAccelBeams.23.042802, 2020.

[6] Benedikt Hermann et al., *Electron beam transverse phase space tomography using nanofabricated wire scanners with submicrometer resolution*, Physical Review Accelerators and Beams, Vol. 24, 022802, DOI: 10.1103/PhysRevAccelBeams.24.022802, 2021.

7 Appendix

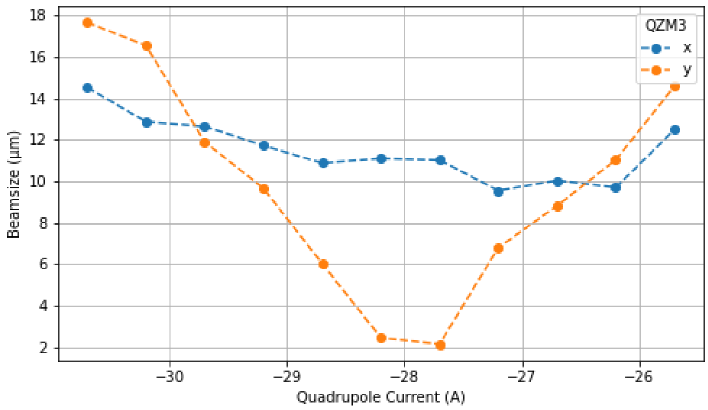
QZM3
x
y
Beamsize (µm)
Quadrupole Current (A)

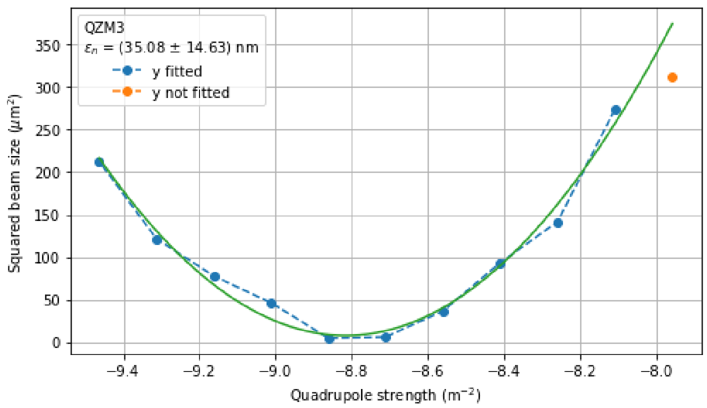
QZM3
ε_n = (35.08 ± 14.63) nm
y fitted
y not fitted
Squared beam size (µm^2)
Quadrupole strength (m^{-2})

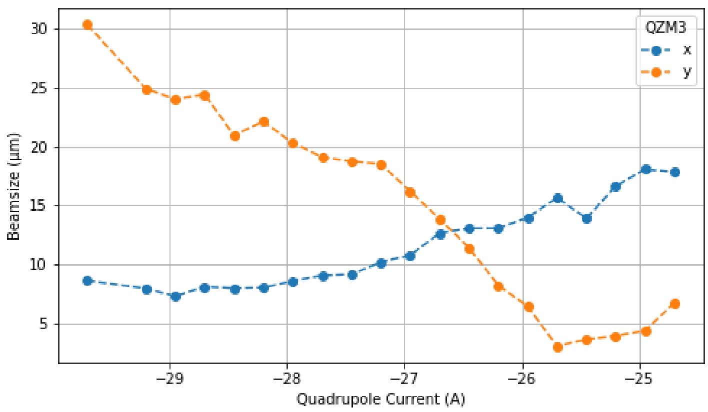
QZM3
x
y
Beamsize (µm)
Quadrupole Current (A)

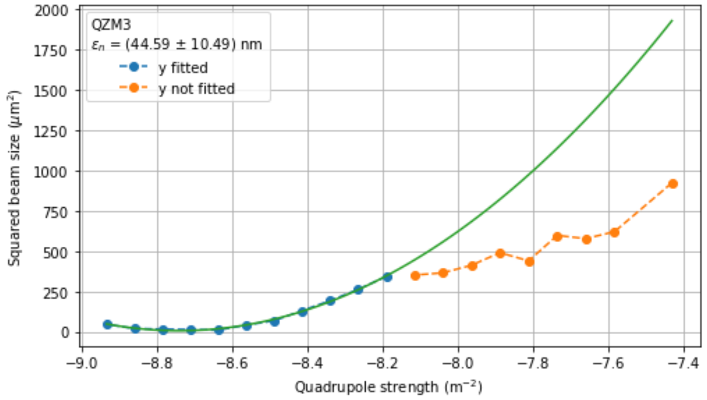
QZM3
ε_n = (44.59 ± 10.49) nm
y fitted
y not fitted
Squared beam size (µm^2)
Quadrupole strength (m^{-2})

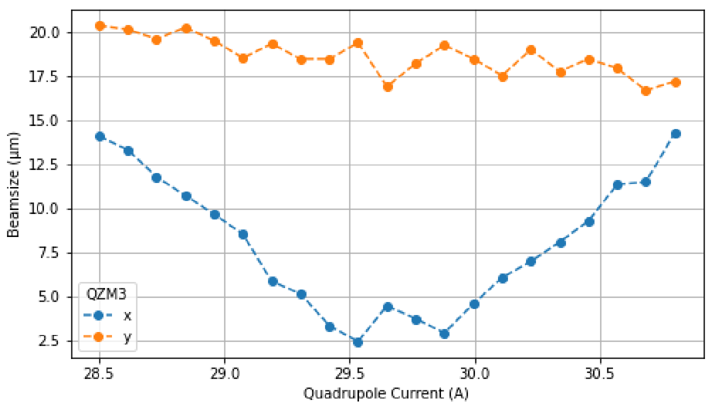
QZM3
x
y
Beamsize (µm)
Quadrupole Current (A)

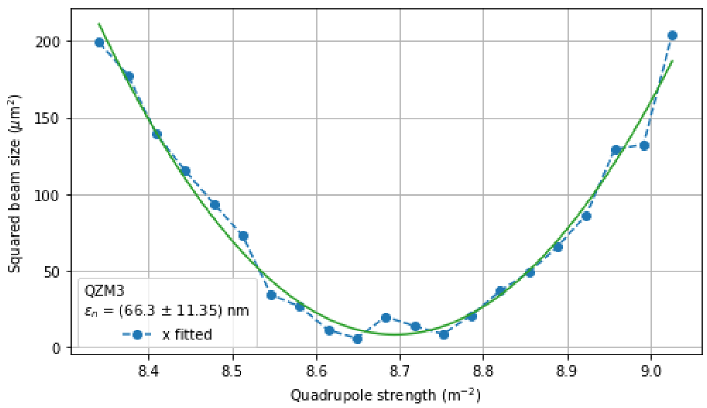
QZM3
ε_n = (66.3 ± 11.35) nm
x fitted
Squared beam size (µm^2)
Quadrupole strength (m^{-2})

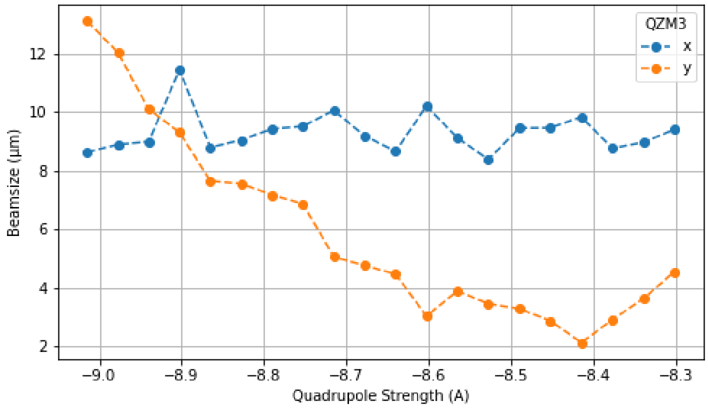
QZM3
x
y
Beamsize (µm)
Quadrupole Strength (A)

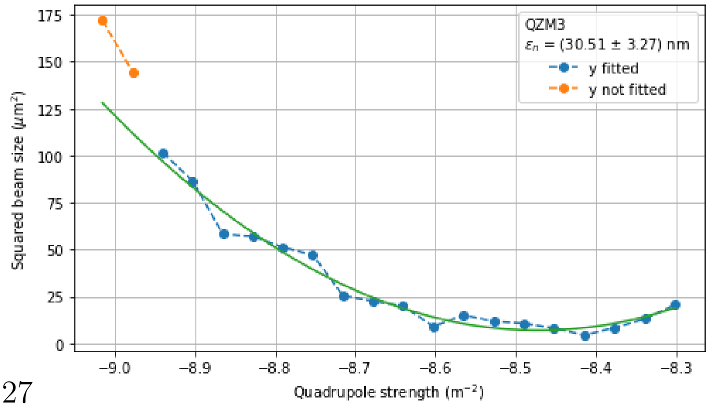
QZM3
ε_n = (30.51 ± 3.27) nm
y fitted
y not fitted
Squared beam size (µm^2)
Quadrupole strength (m^{-2})

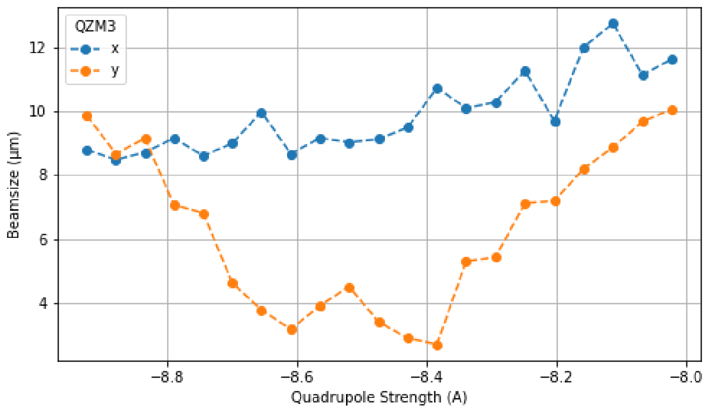
QZM3
x
y
Beamsize (µm)
Quadrupole Strength (A)

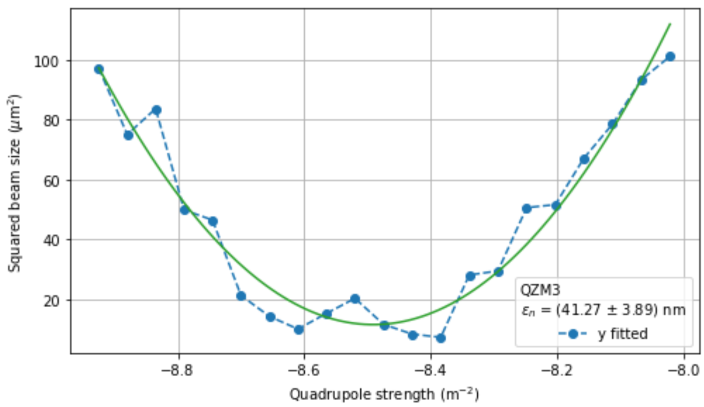
QZM3
ε_n = (41.27 ± 3.89) nm
y fitted
Squared beam size (µm²)
Quadrupole strength (m⁻²)

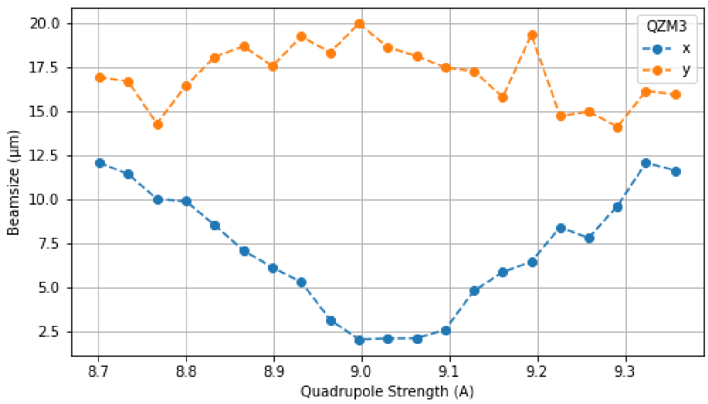
QZM3
x
y
Beamsize (µm)
Quadrupole Strength (A)

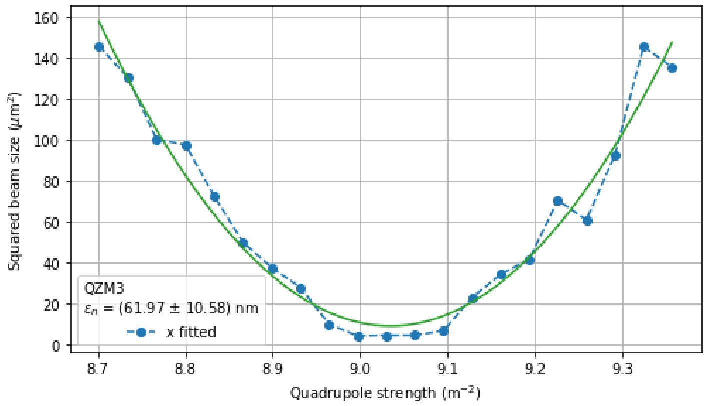
QZM3
ε_n = (61.97 ± 10.58) nm
x fitted
Squared beam size (µm²)
Quadrupole strength (m⁻²)

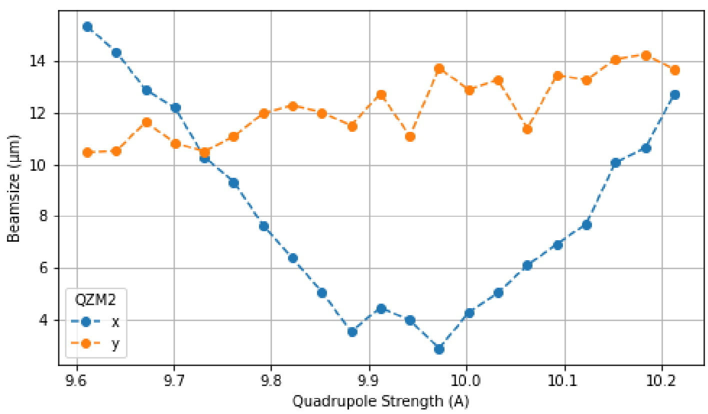
QZM2
x
y
Beamsize (µm)
Quadrupole Strength (A)

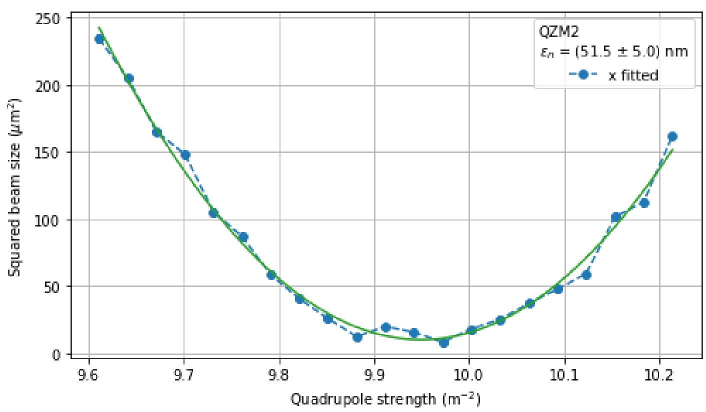
QZM2
ε_n = (51.5 ± 5.0) nm
x fitted
Squared beam size (µm²)
Quadrupole strength (m⁻²)

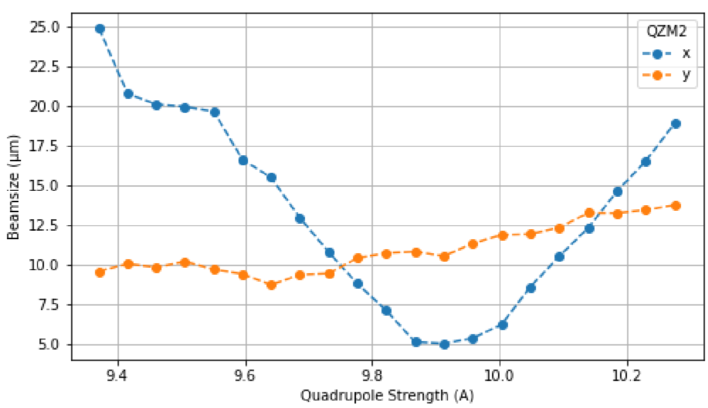
QZM2
x
y
Beamsize (µm)
Quadrupole Strength (A)

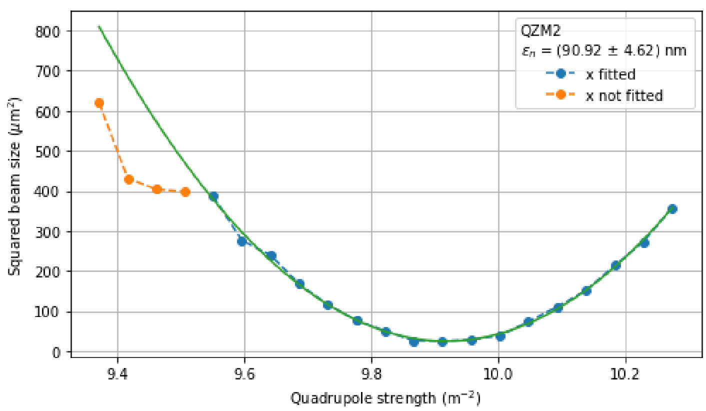
QZM2
ε_n = (90.92 ± 4.62) nm
x fitted
x not fitted
Squared beam size (µm²)
Quadrupole strength (m⁻²)

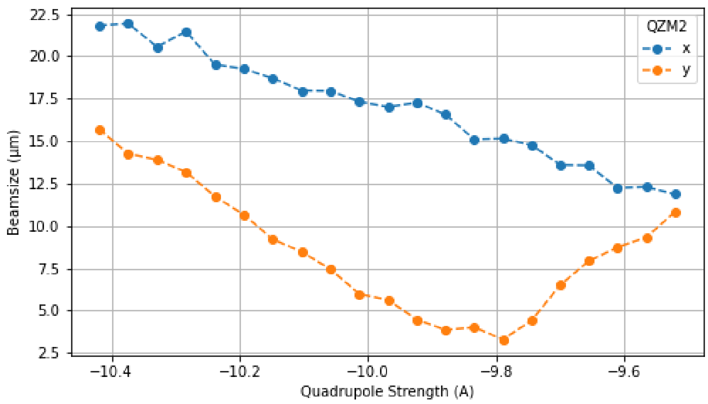
QZM2
x
y
Beamsize (µm)
Quadrupole Strength (A)

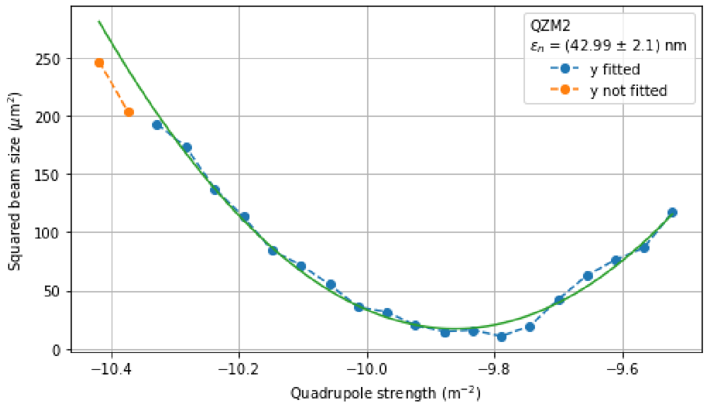
QZM2
ε_n = (42.99 ± 2.1) nm
y fitted
y not fitted
Squared beam size (µm^2)
Quadrupole strength (m^{-2})

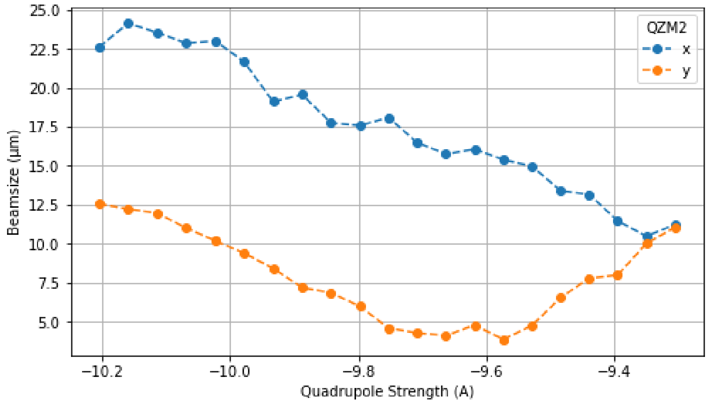
QZM2
x
y
Beamsize (µm)
Quadrupole Strength (A)

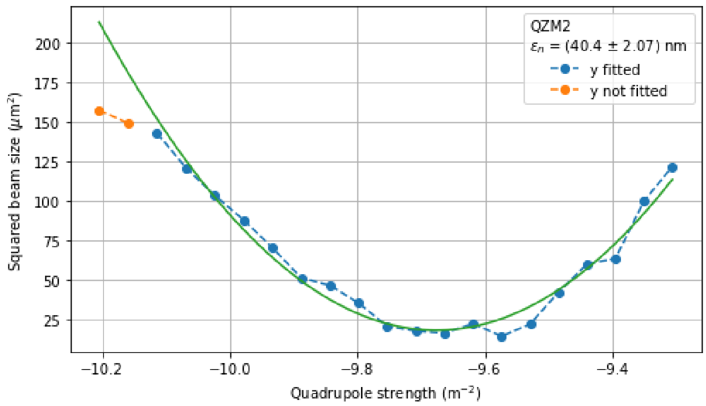
QZM2
ε_n = (40.4 ± 2.07) nm
y fitted
y not fitted
Squared beam size (µm^2)
Quadrupole strength (m^{-2})

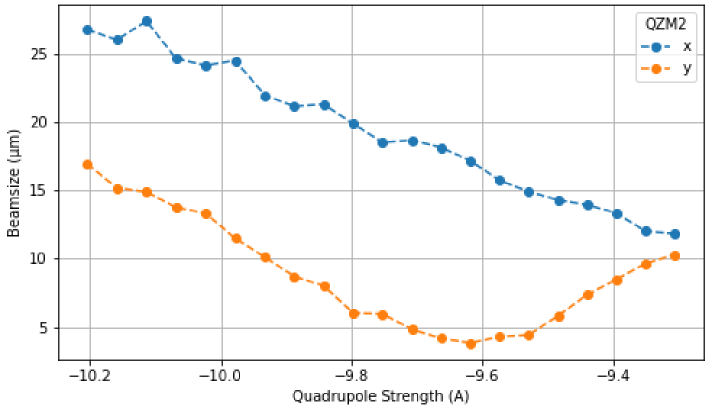
QZM2
x
y
Beamsize (µm)
Quadrupole Strength (A)

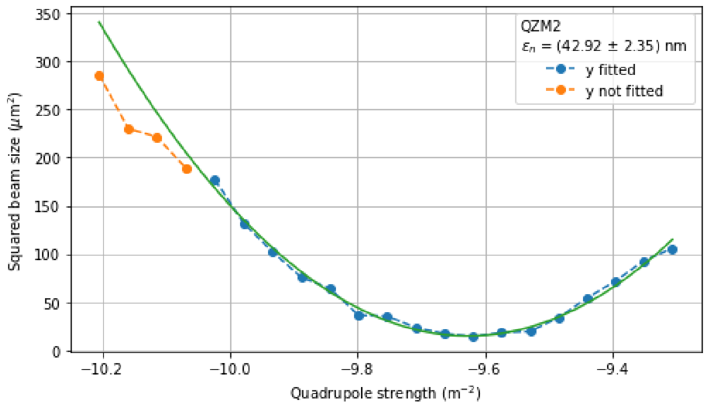
QZM2
ε_n = (42.92 ± 2.35) nm
y fitted
y not fitted
Squared beam size (µm^2)
Quadrupole strength (m^{-2})

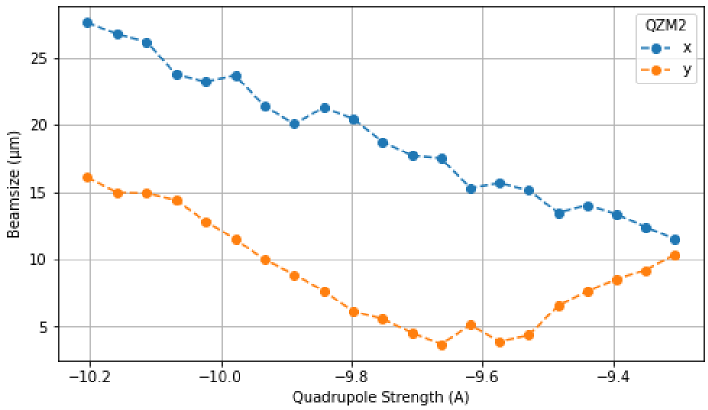
QZM2
x
y
Beamsize (µm)
Quadrupole Strength (A)

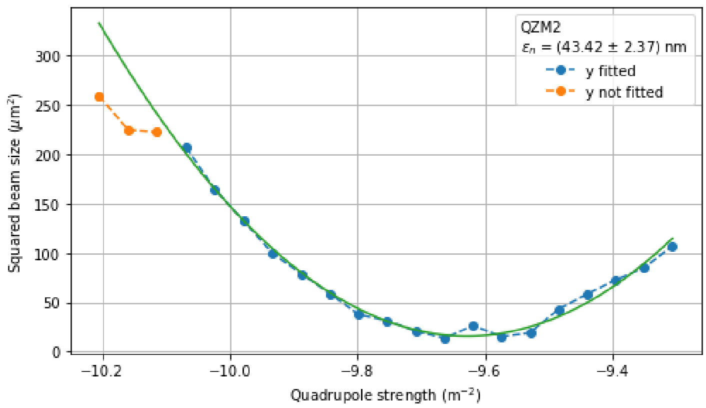
QZM2
ε_n = (43.42 ± 2.37) nm
y fitted
y not fitted
Squared beam size (µm^2)
Quadrupole strength (m^{-2})

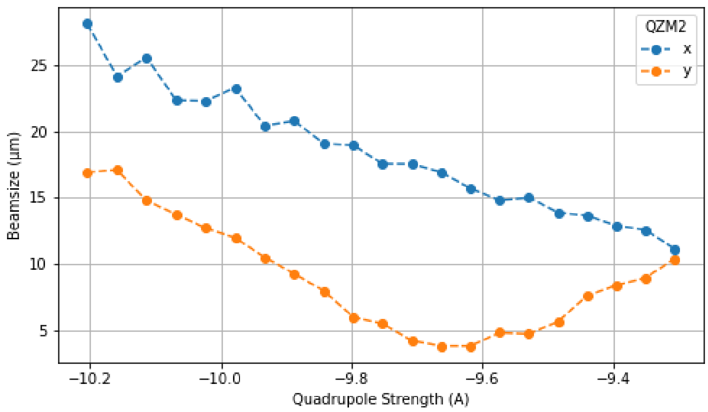
QZM2
x
y
Beamsize (µm)
Quadrupole Strength (A)

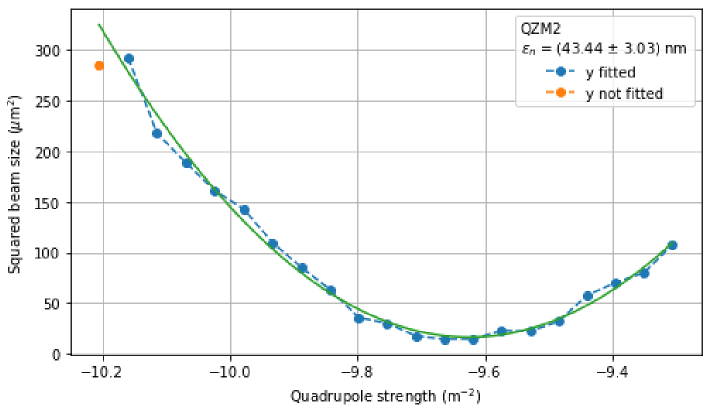
QZM2
ϵ_n = (43.44 ± 3.03) nm
y fitted
y not fitted
Squared beam size (µm²)
Quadrupole strength (m⁻²)

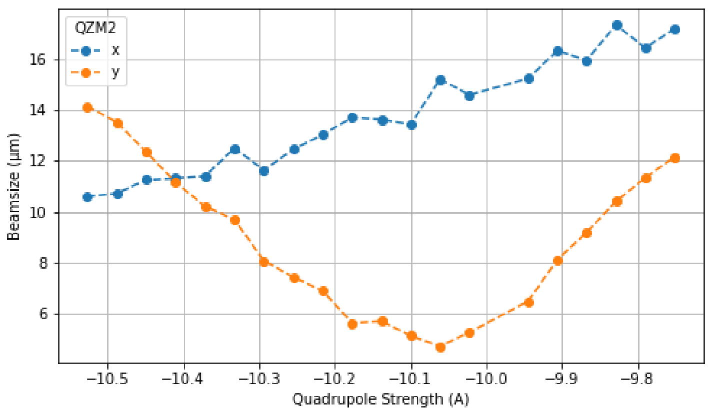
QZM2
x
y
Beamsize (µm)
Quadrupole Strength (A)

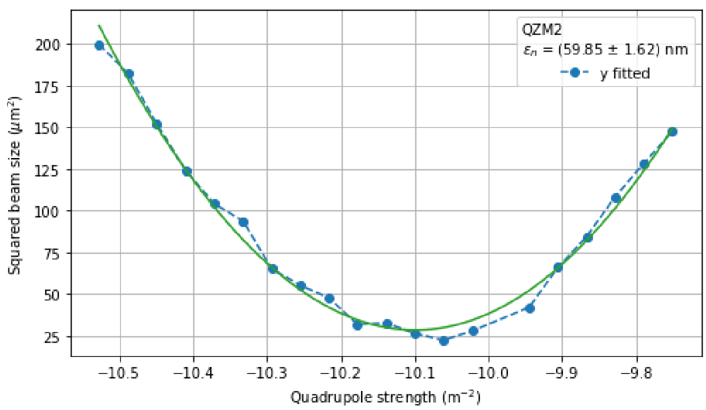
QZM2
ϵ_n = (59.85 ± 1.62) nm
y fitted
Squared beam size (µm²)
Quadrupole strength (m⁻²)

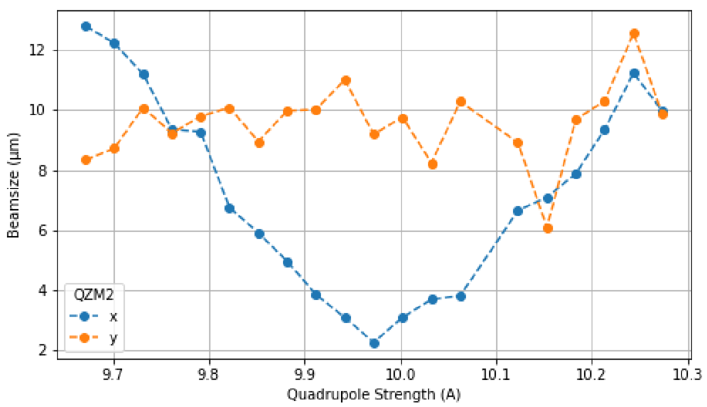
QZM2
x
y
Beamsize (µm)
Quadrupole Strength (A)

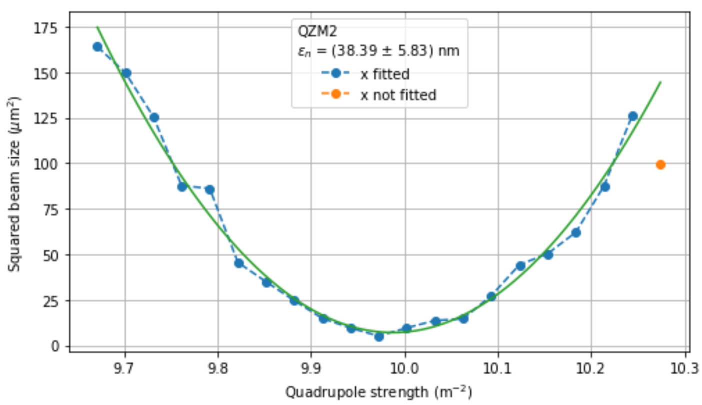
QZM2
ϵ_n = (38.39 ± 5.83) nm
x fitted
x not fitted
Squared beam size (µm²)
Quadrupole strength (m⁻²)